

Short Communication

Improving Resistance to Crack and Corrosion of Laser-Cladded TiC/Co-based Composite Coatings by Doping Minor CeO₂

Chen Wei¹, Yushun Wei¹, Zejun Wang¹, Jianguo Chen^{2*}

¹ Tianjin Special Equipment Inspection Institute, Tianjin 300192, PR China;

² The 18th Research Institute of China Electronics Technology Group Corporation, Tianjin 300384, PR China;

*E-mail: jianguo_chen123@163.com (J. Chen)

Received: 8 February 2022 / Accepted: 21 March 2022 / Published: 7 May 2022

Effects of CeO₂ on the crack resistance and corrosion resistance of TiC/Co-based composite coatings are studied. The microstructure, morphology and element distribution, as well as the phase composition of the coatings were analyzed by optical microscope (OM), scanning electron microscope (SEM) and X-ray diffractometer (XRD), respectively. The results demonstrate that adding a small amount of CeO₂ can make the microstructure of the coating more uniform and effectively improve the crack resistance and corrosion resistance of the coating. The addition of CeO₂ can promote the dissolution of TiC particles in the original powder during laser cladding, and then re-nucleate with CeO₂ as the nucleation sites, producing new refined TiC particles. In addition, the potentiodynamic polarization curves confirmed that with the increase in CeO₂ content, the corrosion potential of the coating increased and the corrosion current decreased, indicating that the corrosion resistance of coating was increased.

Keywords: Composite coating; Crack resistance; Corrosion resistance; Potentiodynamic polarization curve; Microstructure

1. INTRODUCTION

Laser cladding is a promising surface processing way due to its advantages of high input energy, low distortion, minimum dilution between the substrate and the coating, great processing flexibility and the possibility of small area selective cladding. The laser beam can remelt an alloy additives (powder or wire) onto a substrate to achieve the required properties, such as wear resistance, corrosion resistance, high temperature resistance and oxidation resistance, etc. [1-7]. Coating materials usually include Fe-based, Ni-based and Co-based powders. However, in some aggressive environments, only metal powders as coating material cannot meet the actual application requirements,

and it is necessary to add ceramic reinforcement into the metal powder [8-11]. Among various ceramic reinforcements, carbides have the advantages of high hardness, good wear resistance, good corrosion resistance, and good compatibility with the metal matrix, which are the most widely used reinforcement. Although the addition of carbide reinforcement is aimed at improving the surface properties of the coating, it may also cause the formation of defects such as cracks and holes in the coating. Therefore, its application in some special fields is limited [12-14].

In recent years, rare earth CeO_2 has attracted considerable amount of attention, since it can refine the structure and enhance the performance of the metal matrix composite coating [15-18]. Li et al. [19] studied the effect of CeO_2 on microstructure and hardness of NbC reinforced Fe-based composite coatings. It was found that the addition of CeO_2 refined the microstructure and increased the hardness of coatings. Cai et al. [20] investigated the influence of CeO_2 addition on microstructure and properties of TiC reinforced Fe-based cladding layer. The results indicated that the addition of CeO_2 can enhance the micro-hardness and wear resistance of coating. Zhang et al. [21] found that adding appropriate CeO_2 can improve the micro-hardness and corrosion resistance of TiC-VC reinforced Fe-based cladding layer. Liu et al. [22] reported that adding 2 wt.% CeO_2 can lead to the refinement of the microstructure and improve wear resistance of TiC/Ti₂Ni reinforced Ti-based laser cladding composite coating. However, excessive addition of CeO_2 deteriorated the microstructure and wear resistance of coating. Although the effects of CeO_2 addition on microstructure and properties (mainly wear resistance and hardness) of metal matrix composite coating (the vast majority is Fe-based coating) are usually studied, the effect of CeO_2 on microstructure, crack resistance and corrosion resistance of laser clad TiC/Co-based composite coatings has seldom been reported.

This article aims to clarify the role of CeO_2 in regulating the crack resistance and corrosion resistance of laser clad TiC/Co-based composite coatings, which can provide guidance for the application of rare earth in practical engineering coatings.

2. MATERIALS AND EXPERIMENT METHODS

2.1 Preparation of specimens

High Cr ferritic steel with a size of $100 \times 60 \times 20 \text{ mm}^3$ was used as a substrate during laser cladding process. The detailed chemical composition of the substrate is shown in Table 1. The alloy powders are a mixture of HMSP 2528 powder and TiC particles, as well as CeO_2 . HMSP 2528 is a Co-based alloy powder with particle size range of 70-150 μm , and its chemical composition is presented in Table 2. TiC was added into the HMSP 2528 powder (the ratio of TiC and HMSP 2528 is 1:9), and then the high purity CeO_2 was added into the mixed powder of HMSP 2528 powder and TiC with different amounts of 0 wt.%, 0.5 wt.%, and 1.5 wt.%, which were marked as 1#, 2#, and 3#, respectively, as shown in Table 3. The powders were milled by the milling equipment to form completely uniform mixture.

Table 1. Chemical composition of the high Cr ferritic steel in wt.%

C	Cr	W	Mo	Mn	Si	V	Nb	Fe
0.1	8.96	1.5	0.92	0.45	0.32	0.22	0.07	Bal.

Table 2. Nominal chemical composition of Co-based alloy powder (HMSP 2528) in wt.%

C	Cr	Mo	Ni	Fe	Si	Co
0.27	27.6	4.4	2.27	0.5	0.9	Bal.

Table 3. Chemical composition of cladding powders in wt.%

Number	CeO ₂	TiC+ HMSP 2528
1#	0	100
2#	0.5	99.5
3#	1.5	98.5

Fig. 1 shows the schematic diagram of the coating prepared by the laser cladding experiment. Before the laser cladding experiment, a series of SiC papers were used to grind the substrates, and then ultrasonically cleaned with acetone and alcohol. Subsequently, the cladding powders were mixed with alcohol to a concentration close to that of cream and uniformly replaced on the surface of the substrate. The cladding layers were prepared by coating the surface of the substrate with cladding powder using a JK2003SM type Nd: YAG laser equipment. The laser cladding experimental parameters are listed in Table 4.

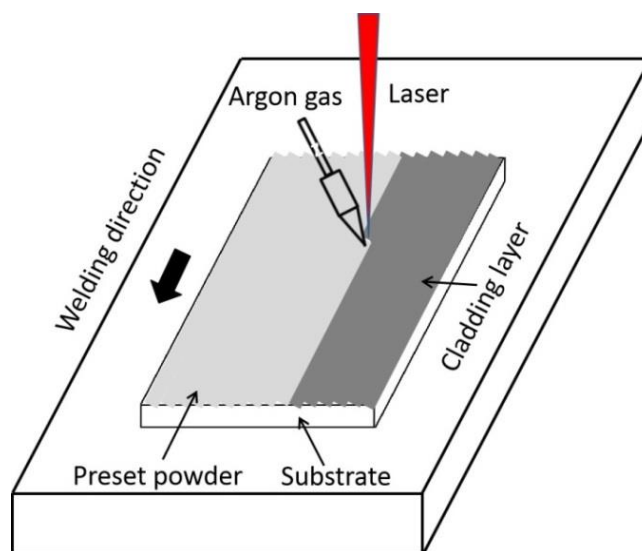


Figure 1. Schematic diagram of the coating prepared by the laser cladding experiment

Table 4. Experimental parameters of laser cladding

Laser output power (W)	Laser beam scanning velocity (mm/min)	Laser beam diameter (mm)	Overlap ratio (%)	Argon flow rate (mL/min)
1800	160	0.7	30	25

2.2 Microstructure analysis

After the laser cladding experiments, the samples were cut from the transversal cross-sections of the coating. The phase constitution of coatings was identified by the Rigaku SmartLab-SE X-ray diffractometer (XRD), with $\text{CuK}\alpha$ radiation over the 2θ range of 20° to 90° at a scanning rate of $20^\circ \text{ min}^{-1}$ (40 kV, 40 mA). Metallographic samples of coatings were grinded using a series of silicon carbide papers followed by polishing and cleaning, and then etched by the nitrohydrochloric acid (the ratio of nitric acid and hydrochloric acid is 1:3). Finally, the etched specimens were placed in alcohol for ultrasonic cleaning, and then dried. The microstructure evolution of coatings was investigated using Olympus DSX510 optical microscope (OM). The corrosion morphology and elements distribution of the composite coatings were studied by S4800 scanning electron microscope (SEM) equipped with energy dispersive spectrometer (EDS).

2.3 Electrochemical measurements

Corrosion resistance of coatings was evaluated by potentiodynamic polarization method. The electrochemical measurement were conducted on an Autolab 302N electrochemical workstation with a three-electrode electrochemical system, namely, a saturated calomel reference electrode, a platinum counter electrode, and the coating as the working electrode. The polarization curves of the laser cladded coatings with different CeO_2 additions were measured in 3.5 wt.% NaCl solution at room temperature. The superficial area of the coatings sample for electrochemical testing was 1cm^2 . During the test of potentiodynamic polarization curves, the scan rate was maintained at 0.5 mV/s.

3. RESULTS AND DISCUSSION

3.1 Phase composition of laser cladding layers

Fig. 2 shows the XRD pattern of laser cladding layers with different CeO_2 contents. It can be found from the figure that the phase composition of the laser cladding layers has no obvious change in the range of CeO_2 addition from 0 to 1.5 wt.%, which are mainly composed of $\gamma\text{-Co}$, Cr_{23}C_6 and TiC. During the laser cladding process, the laser molten pool solidified rapidly, and the $\gamma\text{-Co}$ phase was solidified before the $\gamma \rightarrow \epsilon$ phase transformation occurred. Finally, the $\gamma\text{-Co}$ was retained. The Cr and C in the cladding powder form Cr_{23}C_6 . The TiC in the cladding layers may be the TiC retained in the original cladding powder or the newly generated TiC during the laser cladding process. In addition,

phases containing Ce were not found in the cladding layer, which may be due to the low content of CeO₂ added in cladding powders, and a similar phenomenon was reported in the literature [23].

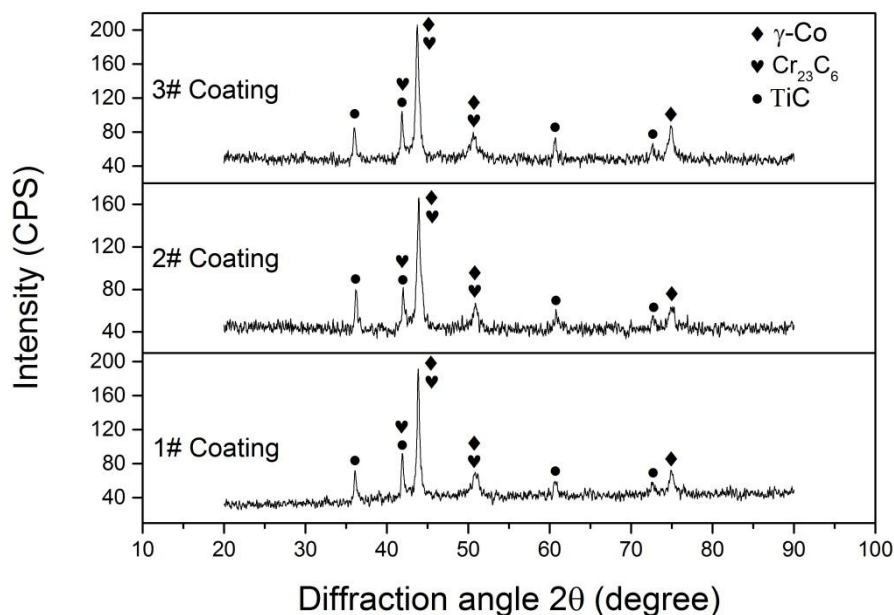


Figure 2. XRD patterns of laser cladding layers with different CeO₂ contents.

3.2 Microstructure of laser cladding layers

Fig. 3 shows the OM of laser cladding coatings with different CeO₂ contents. Firstly, it is found an interesting phenomenon that some large particles existed in the coating with 0 wt.% CeO₂ content, and there are obvious cracks and holes between these large particles, as shown in Fig. 3(a). With the increase of CeO₂ content, these particles gradually become thinner and more uniformly distributed, and cracks and holes are not found in the microstructure, as shown in Fig. 3(b) and Fig. 3(c). Secondly, it can be found that with the increase of CeO₂ content, the grain size of the coating decreases gradually. The grain size of the coatings was measured by the linear intercept method. The result shows the values of grain size for the coatings with different CeO₂ contents of 0 wt.%, 0.5 wt.% and 1.5 wt.% are 9.8 μm, 6.6 μm and 5.1 μm, respectively. The decrease in particle and grain sizes in the coatings caused by the addition of CeO₂ can be explained as follows. On the one hand, CeO₂ acts as heterogeneous nucleation sites in the melting pool owing to its high melting temperature [24]. On the other hand, CeO₂ can reduce surface tension, interfacial energy and critical nucleation energy, thus increasing the number of crystal nuclei [25]. The growth of grain was retarded when more nuclei formed and developed [26].

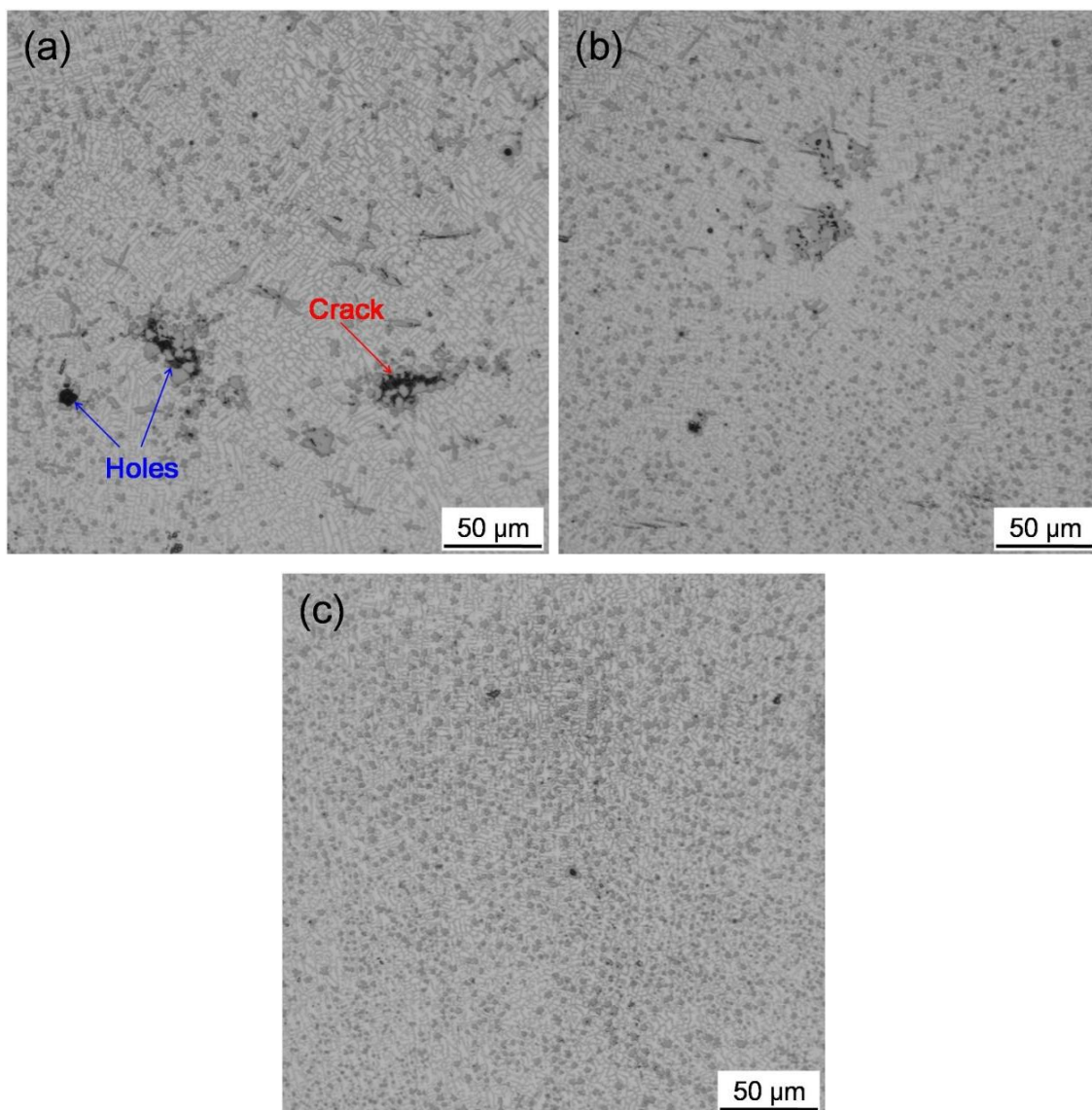


Figure 3. OM images of laser cladding layers with different CeO₂ contents: (a) 0 wt.% CeO₂, (b) 0.5 wt.% CeO₂, (c) 1.5 wt.% CeO₂.

Fig.4 shows the EDS analyses of the precipitated particles and element distribution around the crack and holes in the coating with 0 wt.% CeO₂. As shown in Fig. 4, the distributions of C and Ti were found to be consistent, corresponding to the black particles in the SEM image. Combining the EDS in Fig. 4 and the XRD analysis in Fig. 2, it is found that there are large-sized TiC particles near cracks and holes in the coating without CeO₂ addition. These large-sized TiC particles are the undissolved TiC particles in the original cladding powder. At the same time, the SEM image in Fig. 4 shows that the precipitated particles in the coating without CeO₂ have great difference in size and its distribution is extremely uneven.

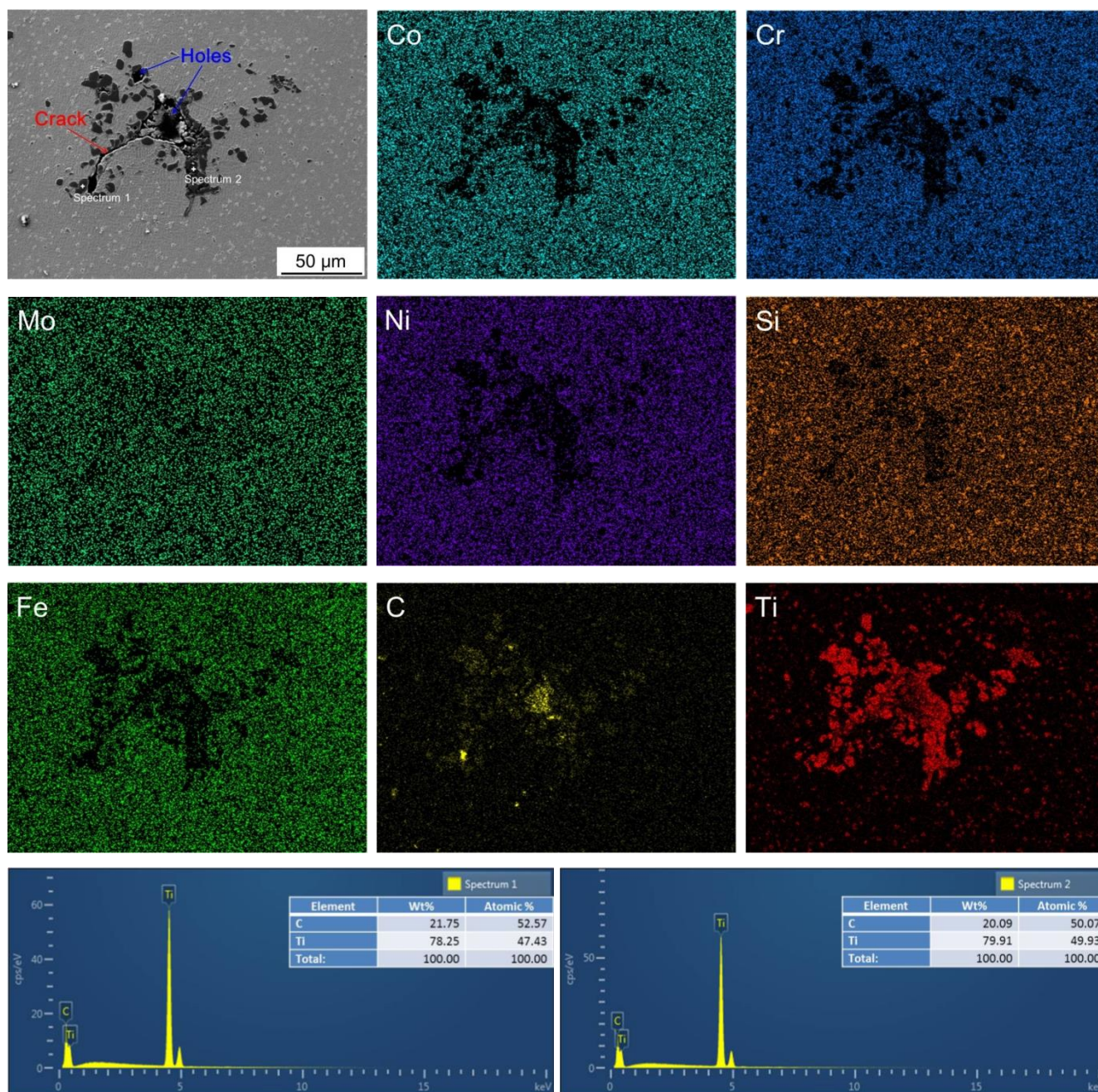


Figure 4. EDS analyses of the precipitated particles and element distribution around the crack and holes in laser cladding layer with 0 wt.% CeO₂.

In order to more clearly observe the element distribution and morphology of small-sized particles in the coating with 0 wt.% CeO₂. Fig.5 shows the EDS analyses of the precipitated particles and element distribution away from the crack and holes in the coating. The results show that the distributions of C and Ti are consistent, which corresponds to the fine precipitated particles in the SEM image. According to the EDS in Fig. 4 and Fig. 5 and the XRD analysis in Fig. 2, the small precipitated particles dispersed in the coating are suggested to be TiC. This further confirmed the formation of new fine TiC particles in the process of laser cladding.

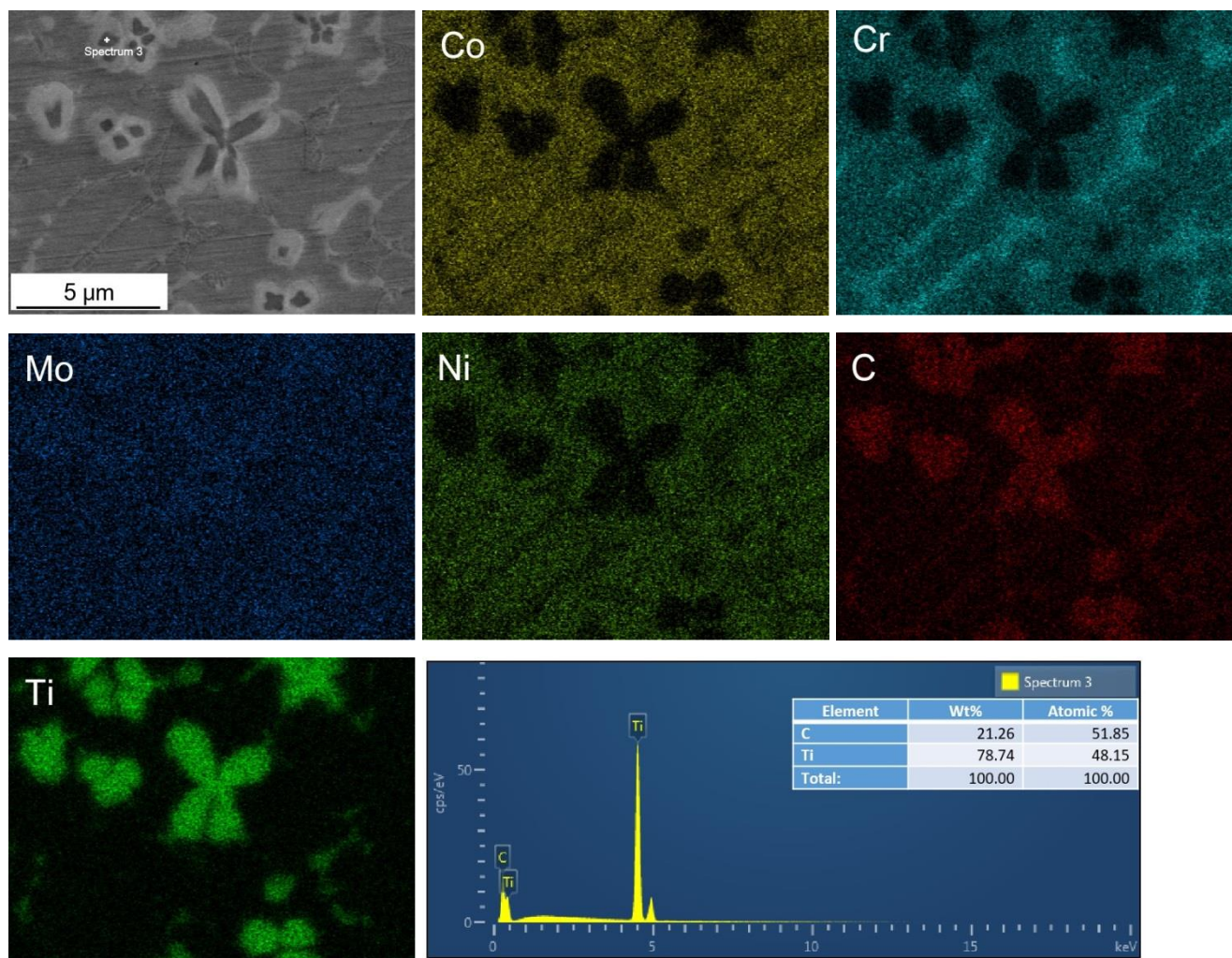


Figure 5. EDS analyses of the precipitated particles and element distribution away from the crack and holes in laser cladding layer with 0 wt.% CeO₂.

Based on the above analysis, there are two forms of TiC in the coating without CeO₂. One is large TiC particles near cracks and holes, and the other is small TiC particles dispersed in the coating. The large TiC particles are the undissolved TiC particles in the original cladding powder, while the small TiC particles are the newly formed precipitates during the laser cladding process.

It is generally suggested that the cracks in the laser cladding process are crucial to the manufacturing and performance reliability of materials. Fig. 4 confirmed that the cracks and holes locate at the large-sized TiC particles caused by the absence of CeO₂. Previous research indicates that the residual stress in the composites dramatically affected crack formation of metal matrix composites by laser cladding [27]. High temperature gradient during laser cladding would lead to the generation of thermal stress in TiC particle. This can be explained by the fact that the thermal expansion coefficient of TiC particle was lower than that of Co matrix. The difference between thermal stress of TiC particle and Co matrix would increase as the size of TiC increases [28]. The larger TiC particles size, the larger interfaces between and TiC and Co matrix, and the larger stress transmitting from interfaces to particles [29]. In addition, the TiC particles with large size were difficult to flow together with Co

matrix during the laser cladding, and they were easy to generate stress concentration [30]. Therefore, the cracks tend to form near the large TiC particles.

Fig.6 shows the EDS line analyses of the precipitated particles nucleation in the coating with 1.5 wt.% CeO₂ addition. It can be seen that the center of the particle is rich in Ce and O elements, corresponding to the black dot in the center of the SEM figure, and other areas of the particle mainly contain Ti and C elements, which indicates that CeO₂ can be used as the nucleation point of the newly formed TiC precipitates in the laser cladding process, promoting the formation of new fine TiC. This can explain that TiC particles in the coating become finer and more uniform with the addition of CeO₂, as shown in Fig. 3.

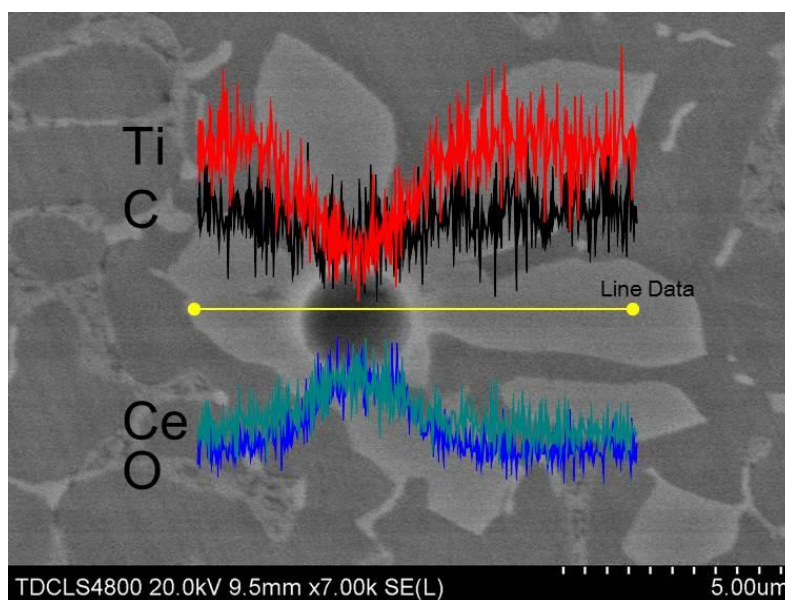


Figure 6. EDS line analyses of the precipitated particle nucleation in laser cladding layer with 1.5 wt.% CeO₂.

3.3 Corrosion resistance of laser cladding layers

Fig. 7 shows the potentiodynamic polarization curves of laser cladding coatings with different CeO₂ contents in 3.5 wt.% NaCl solution. It can be seen that the polarization curves of the three cladding layers show a similar trend, which indicates the similar corrosion mechanism of the coatings. The corrosion current density (i_{corr}) of each coating can be obtained by Tafel extrapolation of both the cathodic and anodic branches of the polarization curve. Table 5 lists the corrosion potentials (E_{corr}) and i_{corr} of the coatings. The data demonstrates that the i_{corr} of the coating decreases with the increase of the CeO₂ content, and the change of the E_{corr} is opposite to that of the i_{corr} . Electrochemical analysis shows that the corrosion resistance of the cladding layer increases with the addition of CeO₂.

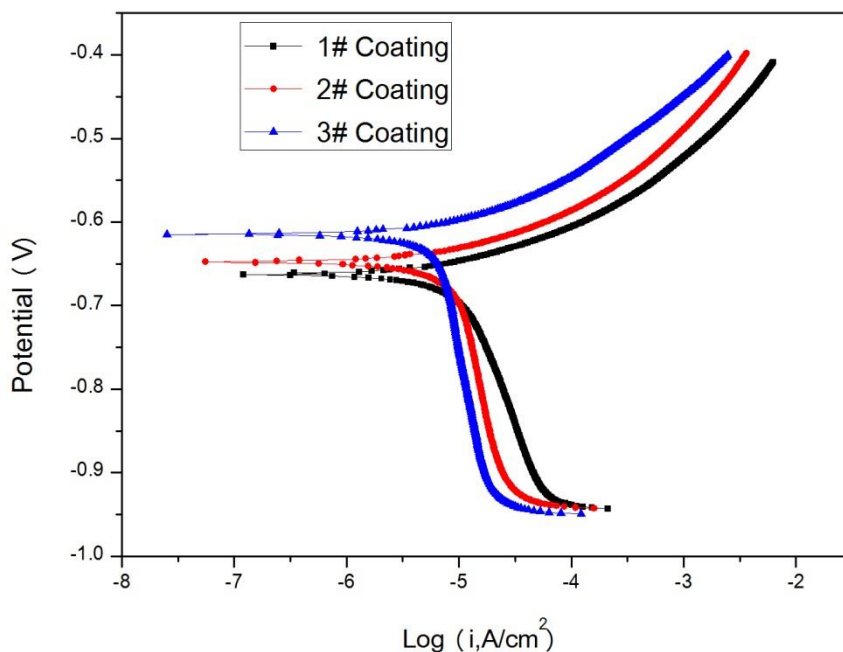


Figure 7. Potentiodynamic polarization curves of laser cladding layers with different CeO₂ contents in 3.5 wt.% NaCl solution: (a) 0 wt.% CeO₂, (b) 0.5 wt.% CeO₂, (c) 1.5 wt.% CeO₂.

Table 5. Electrochemical parameters of coatings in 3.5 wt.% NaCl solution

Number	E _{corr} (V)	I _{corr} (μA/cm ²)
1#	-0.665	3.88
2#	-0.645	3.47
3#	-0.614	3.14

Fig. 8 shows the SEM micrographs of the laser cladding coatings with different CeO₂ contents after immersion in 3.5 wt.% NaCl solution for 30 days. It can be seen that the corrosion phenomenon of coatings gradually disappeared with the increase of CeO₂ content, which is consistent with the results of potentiodynamic polarization test. The difference in corrosion resistance is due to the different size and distribution of precipitated particles [31]. The coating with 0 wt.% CeO₂ has the worst corrosion resistance, as shown in fig.8 (a), due to the large size difference and uneven distribution of TiC. And there are obvious cracks and holes around the large-sized TiC, which will increase the possibility of pitting corrosion and gap corrosion of the coating. The corrosion resistance of the coating becomes stronger with the increase of CeO₂ content. Although the coating containing 0.5 wt.% CeO₂ shows slight signs of corrosion, the coating containing 1.5 wt.% CeO₂ almost exhibit no corrosion, as shown in fig.8 (b) and fig.8 (c). The increase of CeO₂ not only eliminates the cracks of the coating, but also refines the size of TiC in the coating and homogenizes the size of TiC. The

absence of cracks will greatly improve the corrosion resistance of the coating, because the corrosive medium cannot easily enter the interior of the coating. Fine and evenly distributed TiC particles can reduce the tendency of local pitting corrosion of the coating. Previous similar study [32] also confirmed that TiC with small-sized and high concentration can improve the corrosion resistance of the in TiC/TiAl composite coating. In addition, it is worth noting that excessive addition of CeO₂ will deteriorate the performance of the coating [33].

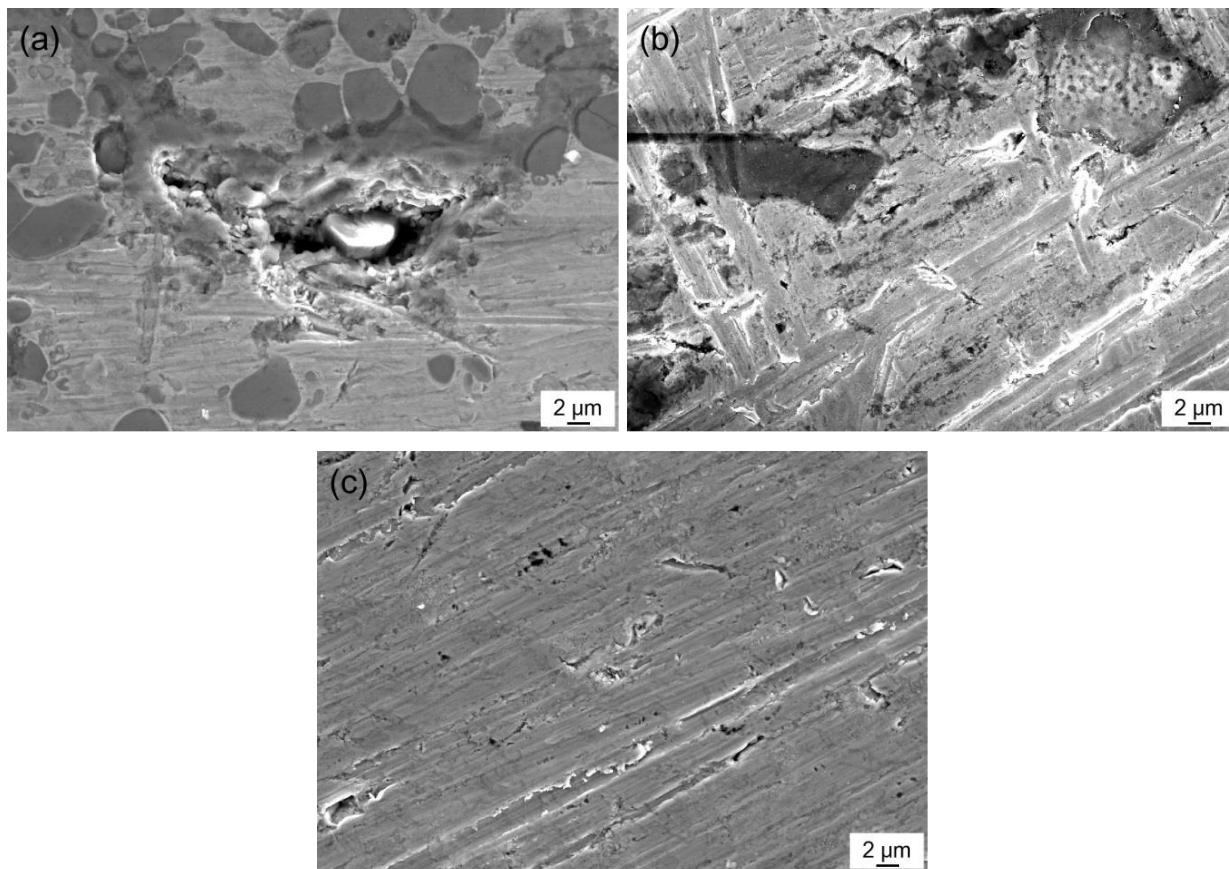


Figure 8. SEM micrographs of corrosion morphology of the laser cladding layers with different CeO₂ contents after immersion in 3.5 wt.% NaCl solution for 30 days: (a) 0 wt.% CeO₂, (b) 0.5 wt.% CeO₂, (c) 1.5 wt.% CeO₂.

4. CONCLUSIONS

In this work, the effects of CeO₂ addition from 0 wt.% to 1.5 wt. % on microstructure, crack resistance and corrosion resistance of laser clad TiC/Co-based composite coatings have been studied. The following conclusions can be drawn:

(1) In the range of CeO₂ addition from 0 wt.% to 1.5 wt. %, the laser cladding layers are composed of γ -Co, TiC, and Cr₂₃C₆ phases.

(2) The grain size of the laser cladding layer is refined from 9.8 μ m to 5.1 μ m with the increase of CeO₂ content from 0 wt.% to 1.5 wt. %.

(3) Obvious cracks and holes will be formed around the unmelted large-sized TiC in the coating containing 0 wt.% CeO₂ during laser cladding.

(4) CeO₂ can be used as the nucleation point of newly generated TiC during laser cladding process.

(5) The addition of CeO₂ can make the distribution of TiC in the coating more uniform and refine the size of TiC, and then prevent the formation of cracks and holes.

(6) Addition of CeO₂ can improve the crack resistance and corrosion resistance of the laser cladding layers.

ACKNOWLEDGEMENTS

This work was financially supported by the Science and Technology Program of Tianjin Administration for Market Regulation (No. 2021-W23). Thanks to partial support for this work from National Detection and inspection Center for Special Equipment Welding consumables quality (Tianjin).

CONFLICTS OF INTEREST

The authors declare that they have no known competing interests that could have appeared to influence the work reported in this paper.

DATA AVAILABILITY STATEMENT

All data generated or analyzed during this work are included within the article.

References

1. J.L Liu, H.J Yu, C.Z Chen, F. Weng and J.J Dai, *Opt. Laser. Eng.*, 93 (2017) 195.
<https://doi.org/10.1016/j.optlaseng.2017.02.007>
2. F. Weng, C.Z. Chen and H.J. Yu, *Mater. Design.* 58 (2014) 412.
<https://doi.org/10.1016/j.matdes.2014.01.077>
3. K. Feng, Y. Chen, P. Deng, Y. Li, H. Zhao, F. Lu, R. Li, J. Huang and Z. Li, *J. Mater. Process. Technol.*, 243 (2017) 82.
<https://doi.org/10.1016/j.jmatprotec.2016.12.001>
4. Z. Zhang, R. Kovacevic, *J. Manuf. Process.*, 38 (2019) 63.
<https://doi.org/10.1016/j.jmapro.2019.01.001>
5. Z.P. Hu, Z.F. Du, Z.W. Yang, L.M. Yu and Z.Q. Ma, *Mater. Sci. Eng. A*, 836 (2022) 142740.
<https://doi.org/10.1016/j.msea.2022.142740>
6. S.Q. Xia, Z.X. Xia, D. Zhao, Y. Xie, X. Liu and L. Wang, *Fusion Eng. Des.*, 172 (2021) 112792.
<https://doi.org/10.1016/j.fusengdes.2021.112792>
7. Z.X. Xia, J.C. Xu, J.J. Shi, T. Shi, C.F. Sun and D. Qiu, *Addit. Manuf.*, 33 (2020) 101114.
<https://doi.org/10.1016/j.addma.2020.101114>
8. Y. Hu, W. Cong, *Ceram. Int.*, 44 (2018) 20599.
<https://doi.org/10.1016/j.ceramint.2018.08.083>
9. Y.Q. Ren, L.Q. Li, Y.D. Zhou and S.L. Wang, *Mater. Lett.*, 315 (2022) 131962.
<https://doi.org/10.1016/j.matlet.2022.131962>
10. Y.C. Cai, Z. Luo, M.N. Feng, Z.M. Liu, Z.Y. Huang and Y.D. Zeng, *Surf. Coat. Technol.*, 291 (2016) 222.

- <https://doi.org/10.1016/j.surfcoat.2016.02.033>
11. L.Q. Li, J.D. Wang, P.P. Lin and H. Liu, *Ceram. Int.*, 43 (2017) 16638.
<https://doi.org/10.1016/j.ceramint.2017.09.054>
 12. S. Zhou, X. Zeng, Q. Hu and Y. Huang, *Appl. Surf. Sci.*, 255 (2008) 1646.
<https://doi.org/10.1016/j.apsusc.2008.04.003>
 13. S.K. Ghosh, P. Saha, *Mater. Design.* 32 (2011) 139.
<https://doi.org/10.1016/j.matdes.2010.06.020>
 14. Q. Wang, Q. Li, L. Zhang, D. Chen, H. Jin, J. Li, J. Zhang and C. Ban, *Ceram. Int.*, 48 (2022) 7905.
<https://doi.org/10.1016/j.ceramint.2021.11.338>
 15. S.T. Sun, H.G. Fu, X.L. Ping, X.Y. Guo, J. Lin, Y.P. Lei, W.B. Wu and J.X. Zhou, *Surf. Coat. Technol.*, 359 (2019) 300.
<https://doi.org/10.1016/j.surfcoat.2018.12.083>
 16. J.G. Chen, Q.S. Li, B. Sun, Q.H. Zhao, Z.J. Wang, W.F. Niu, X. Wang, L.H. Dang and Q.J. Ma, *Int. J. Electrochem. Sci.*, 16 (2021) 210511.
<https://doi.org/10.20964/2021.05.10>
 17. Y.C. Cai, Z. Luo and Y. Chen, *High Temp. Mater. Proc.*, 37 (2017) 209.
<https://doi.org/10.1515/htmp-2016-0198>
 18. G.Y. Han, Y.F. Zhang, B. Wang and Z.X. Zhang, *Int. J. Electrochem. Sci.*, 16 (2021) 210255.
<https://doi.org/10.20964/2021.02.04>
 19. Q. Li, Y. Lei and H. Fu, *Surf. Coat. Technol.*, 239 (2014) 102.
<https://doi.org/10.1016/j.surfcoat.2013.11.026>
 20. Y.C. Cai, Z. Luo, Y. Chen and S.S. Ao, *Surf. Eng.*, 33(2017) 936.
<https://doi.org/10.1080/02670844.2017.1309742>
 21. H. Zhang, Y. Zou, Z.D. Zou and D.T. Wang, *J. Alloys Compd.*, 622 (2015) 62.
<https://doi.org/10.1016/j.jallcom.2014.10.012>
 22. Y.N. Liu, R.L. Sun, W. Niu, T.G. Zhang and Y.W. Lei, *Opt. Laser Eng.*, 120 (2019) 84.
<https://doi.org/10.1016/j.optlaseng.2019.03.001>
 23. Y. Fan, G. Jin, X.F. Cui, Y. Li and Z.H. Gao, *Surf. Coat. Technol.*, 288 (2016) 25.
<https://doi.org/10.1016/j.surfcoat.2016.01.007>
 24. M.X. Li, S.H. Zhang, H.S. Li, Y.Z. He, J.H. Yoon and T.Y. Cho, *J. Mater. Process. Technol.*, 202 (2008) 107.
<https://doi.org/10.1016/j.jmatprotec.2007.08.050>
 25. L. Ding, S.S. Hu, *Surf. Coat. Technol.*, 276 (2015) 565.
<https://doi.org/10.1016/j.surfcoat.2015.06.014>
 26. X. Zhou, G. Liu, X. Shen, and Y. Liu, *Mater. Sci. Eng. A*, 829 (2022) 142071.
<https://doi.org/10.1016/j.msea.2021.142071>
 27. P.B. Kadolkar, T.R. Watkins, J.Th.M. De Hosson, B.J. Kooi and N.B. Dahotre, *Acta Mater.*, 55 (2007) 1203.
<https://doi.org/10.1016/j.actamat.2006.07.049>
 28. Farida Bouafia, Boualem Serier and Bel Abbas BachirBouiadjra, *Comp. Mater. Sci.*, 54 (2012) 195.
<https://doi.org/10.1016/j.commatsci.2011.10.030>
 29. J.D. Wang, L.Q. Li and W. Tao, *Opt. Laser Technol.*, 82 (2016) 170.
<https://doi.org/10.1016/j.optlastec.2016.03.008>
 30. J.D. Wang, L.Q. Li, P.P. Lin and J.M. Wang, *Opt. Laser Technol.*, 105 (2018) 195.
<https://doi.org/10.1016/j.optlastec.2018.03.009>
 31. Q.M. Liang, W. Wang, Z.S. Chen and W.M. Lin, *Int. J. Electrochem. Sci.*, 16 (2021) 210647.
<https://doi.org/10.20964/2021.06.28>
 32. X. He, R.G. Song and D.J. Kong, *Opt. Laser Technol.*, 112 (2019) 339.
<https://doi.org/10.1016/j.optlastec.2018.11.037>

33. H. Zhang, Y. Zhou, Z. Zou and C. Shi, *J. Rare. Earth.*, 32 (2014) 1095.
[https://doi.org/10.1016/S1002-0721\(14\)60188-5](https://doi.org/10.1016/S1002-0721(14)60188-5)

© 2022 The Authors. Published by ESG (www.electrochemsci.org). This article is an open access article distributed under the terms and conditions of the Creative Commons Attribution license (<http://creativecommons.org/licenses/by/4.0/>).